How to cite: *Angew. Chem. Int. Ed.* **2022,** *61,* e202209947
International Edition: doi.org/10.1002/anie.202209947
German Edition: doi.org/10.1002/ange.202209947

Photoaffinity Labeling

Developing Isoxazole as a Native Photo-Cross-Linker for Photoaffinity Labeling and Chemoproteomics

Ke Cheng, Junyang Qi, Xiaojie Ren, Jie Zhang, Huangxu Li, Hanyue Xiao, Rui Wang, Zhiyang Liu, Lingkuan Meng, Nan Ma, and Hongyan Sun**

Abstract: Photoaffinity labeling is a powerful technique to interrogate drug-protein interactions in native cellular environments. Photo-cross-linkers are instrumental for this technique. However, the introduction of unnatural photo-cross-linkers may significantly reduce the bioactivity of the drug, thus impairing the chemoproteomic outcomes. Herein, we developed a common pharmacophore, isoxazole, into a natively embedded photo-cross-linker for chemoproteomics, which minimally perturbs the drug structure. The photo-cross-linking reactions of the isoxazole were thoroughly investigated for the first time. Functionalized isoxazoles were then designed and applied to protein labeling, demonstrating the superior photo-cross-linking efficiency. Subsequently, two isoxazole-based drugs, Danazol and Luminespib, were employed in chemoproteomic studies, revealing their potential cellular targets. These results provide valuable strategies for future chemoproteomic study and drug development.

Introduction

Photoaffinity labeling (PAL) using photo-cross-linkers has been developing rapidly over the past decades[1] and provides a powerful and versatile tool for interactome mapping in native cellular environments.[2] Upon photoactivation, highly reactive species such as carbene, nitrene, and free radicals are produced from photo-cross-linkers and cross-linked to biomolecules instantly via covalent bonds. To date, aryl-azide, benzophenone, and diazirine are the three major photo-cross-linkers, owing to their unique photochemistry (Figure 1A). Among these photo-cross-linkers, diazirine has become the most popular in chemoproteomic studies due to its compact size, long activating wavelength, and superior photoreactivity.[3] Notably, Yao's group has developed the "minimalist" diazirine linkers,[4] which were widely utilized in recent chemoproteomic studies.[2a–e]

Despite their widespread application, a major problem remains with these photo-cross-linkers: the bioactivity of the

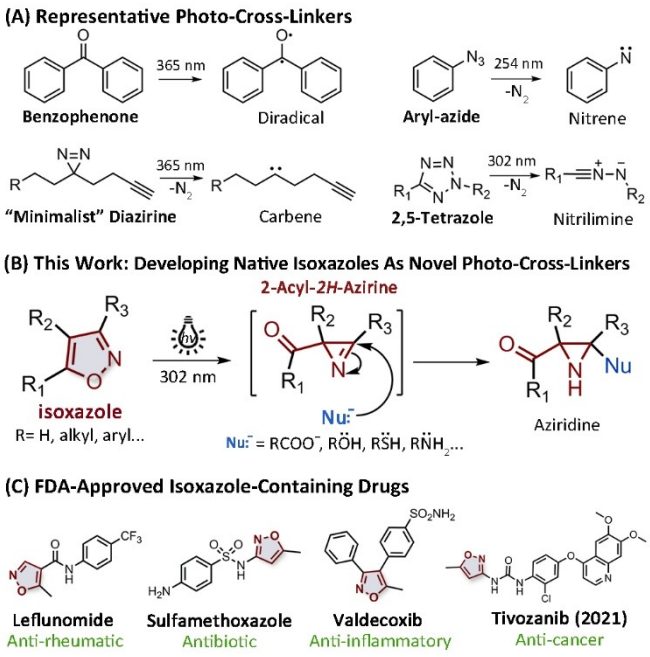

Figure 1. A) Overview of major photo-cross-linkers in recent chemoproteomic studies. B) Developing isoxazoles as novel photo-cross-linkers in this study. C) Representative FDA-approved isoxazole-containing drugs.

[*] Dr. K. Cheng, Dr. X. Ren, Dr. J. Zhang, H. Li, H. Xiao, Z. Liu, L. Meng, Prof. H. Sun
Department of Chemistry and COSDAF (Center of Super-Diamond and Advanced Films), City University of Hong Kong
Hong Kong SAR (China)
E-mail: hongysun@cityu.edu.hk
Prof. N. Ma
Center for Bioactive Natural Molecules and Innovative Drugs Research, College of Pharmacy, Jinan University
Guangzhou 510632 (China)
E-mail: nanma927@126.com
Dr. K. Cheng, Dr. J. Qi
School of Pharmaceutical Sciences (Shenzhen), Shenzhen Campus of Sun Yat-sen University
Shenzhen 518107 (China)
Dr. R. Wang
Pingshan Translational Medicine Center, Shenzhen Bay Laboratory
Shenzhen, 518118 (China)
Prof. N. Ma
JNU-HKUST Joint Laboratory for Neuroscience and Innovative Drug Research, College of Pharmacy, Jinan University
Guangzhou 510632 (China)

drug/ligand is often attenuated when an unnatural photo-cross-linker is introduced. Developing natively embedded photo-cross-linkers can effectively solve this problem. In a seminal work, Yao et al. discovered that tetrazole could efficiently react with various biological nucleophiles under UV irradiation, making it a highly useful photo-cross-linker[5] (Figure 1A). Owing to its bioisostere property, tetrazole is commonly utilized as a pharmacophore in drug discovery.[6] In later studies, Li and co-works directly used the tetrazole moiety as a natively embedded photo-cross-linker for protein labeling and chemoproteomic studies.[7] In another work, Sieber's group successfully uncovered the cellular targets of a natural product, elegaphenone, utilizing the photoreactivity of a natively embedded benzophenone group.[8] Without introducing extra photo-cross-linkers, this strategy can retain most bioactivity of the probe and greatly facilitate the subsequent chemoproteomic studies.

Inspired by these achievements, we endeavored to develop novel photoreactive pharmacophores to further expand the chemical toolbox for photoaffinity labeling. One of the frequently used pharmacophores, isoxazole, caught our strong attention due to its intriguing properties, such as good solubility, bio-compatibility, and photoreactivity. The photolysis of isoxazole was first reported in 1966 and reinvestigated lately.[9] Due to the weak N–O bond, the isoxazole ring tends to collapse under UV irradiation, rearranging to oxazole through azirine intermediate. Meanwhile, the reactions of azirine with different nucleophiles were reported, especially its reaction with carboxylic acid, which has been recently used for bioconjugation and protein labeling.[10] Based on these reactions, we proposed that isoxazoles could be photo-cross-linked with biomolecules through the azirine intermediates, as shown in Figure 1B.

Isoxazole moiety is frequently found in bioactive compounds and drugs due to its interactions with biomolecules via hydrogen bond and π-π stacking effect.[11] Notably, dozens of isoxazoles have been approved by the United States Food and Drug Administration (USFDA) (Figure 1C), including Valdecoxib, Micafungin, and Tivozanib, a novel kinase inhibitor approved in 2021. Meanwhile, numerous new isoxazoles were developed over the decades as anticancer drugs, anti-inflammatory agents, and antibiotics.[12] Hence, developing isoxazole as a natively embedded photo-cross-linker can provide a practical approach for chemoproteomic studies of isoxazole-containing drugs and aid in drug discovery.

In this study, we reported the development of a common pharmacophore, isoxazole, into a novel photo-cross-linker for chemoproteomics. First, the photoreactions of isoxazole with amino acids/peptides/proteins were thoroughly studied. Then, functionalized isoxazole probes with different substituents were designed for in vitro/situ labeling to demonstrate their superior photo-cross-linking efficiency. Further chemoproteomic experiments with two isoxazole-based drugs, Danazol and Luminespib, revealed their potential cellular targets and interactions. In addition, the covalent inhibition of Luminespib towards heat shock protein 90 (Hsp90) under UV irradiation was also investigated.

Results and Discussion

To verify the photoreaction of isoxazoles, a simple isoxazole, methyl 5-phenylisoxazole-3-carboxylate (**MPISC**), was used as a model molecule. The UV absorption of **MPISC** was first measured, and a broad absorption (260–310 nm) was observed (Figure S2). Considering that short-wave UV may damage cells and proteins, a 302 nm handheld UV lamp (6 W) was used as the photo trigger. **MPISC** was first investigated for its photoreactivity towards single amino acids. Based on previous studies,[10] a highly active azirine intermediate could be generated from the photolysis of **MPISC**. The azirine can then react with amino acids through nucleophilic addition, affording aziridine as the final product (Figure 2A). Density functional theory (DFT) calculations were performed to investigate the reaction coordinates of the azirine intermediate with different nucleophiles (carboxyl acid, amine, and thiol). As shown in Figure 2B, azirine could react with acetic acid through a transition state with a relatively low activation energy barrier. Subsequently, the aziridine was generated with low free energy, suggesting a smooth cross-linking process and high stability of the photo-cross-linking products. Meanwhile, DFT calculations of the azirine intermediate with amine/thiol also demonstrated energetically favorable reaction coordinates (Figure S3). These DFT calculations suggested that all three nucleophiles could react with the azirine intermediate.

The photoreactions of **MPISC** and carboxylic acids, including glutamic acid (Z-Glu-OMe) and acetic acid, were analyzed by HPLC. As expected, **MPISC** reacted rapidly with Z-Glu-OMe or acetic acid within 5 min, and the aziridine products (**AZD1** & **AZD2**) were produced with high yields (Figure 2C & Figure S5). No azirine intermediate was detected during the process, implying its high reactivity with carboxylic acids. The aziridine products, **AZD1** and **AZD2**, were successfully isolated and characterized by high-resolution mass spectrometry (HRMS) and NMR (Supporting Information), thus confirming our hypothesis. Moreover, **AZD1** showed excellent stability under ambient conditions (Figure S6). The photoreactions of **MPISC** with other common nucleophilic amino acids, including tyrosine, cysteine, and lysine, were also investigated by HPLC and HRMS. The results demonstrated that **MPISC** could also be successfully photo-cross-linked to these nucleophilic amino acids upon UV irradiation (Figure S7–S9). However, the photoreaction yields were relatively low compared with that with carboxylic acid, probably due to side reactions. Taken together, these results together suggested that the photoreaction of isoxazole can be potentially applied to protein labeling and chemoproteomics.

After verifying the photoreaction with single amino acids, **MPISC** was tested for its photoreaction with a free peptide containing diverse residues (RQYAWESGFTCNHK). Peptides with modifications of 1 and 2 **MPISC** were detected by MALDI-TOF MS (matrix-assisted laser desorption-ionization time of flight mass spectrometry) analysis (Figure S10), indicating the photo-cross-linking on the peptide by **MPISC**. The modification sites on the peptide were further characterized by LC–MS/MS. Glutamic

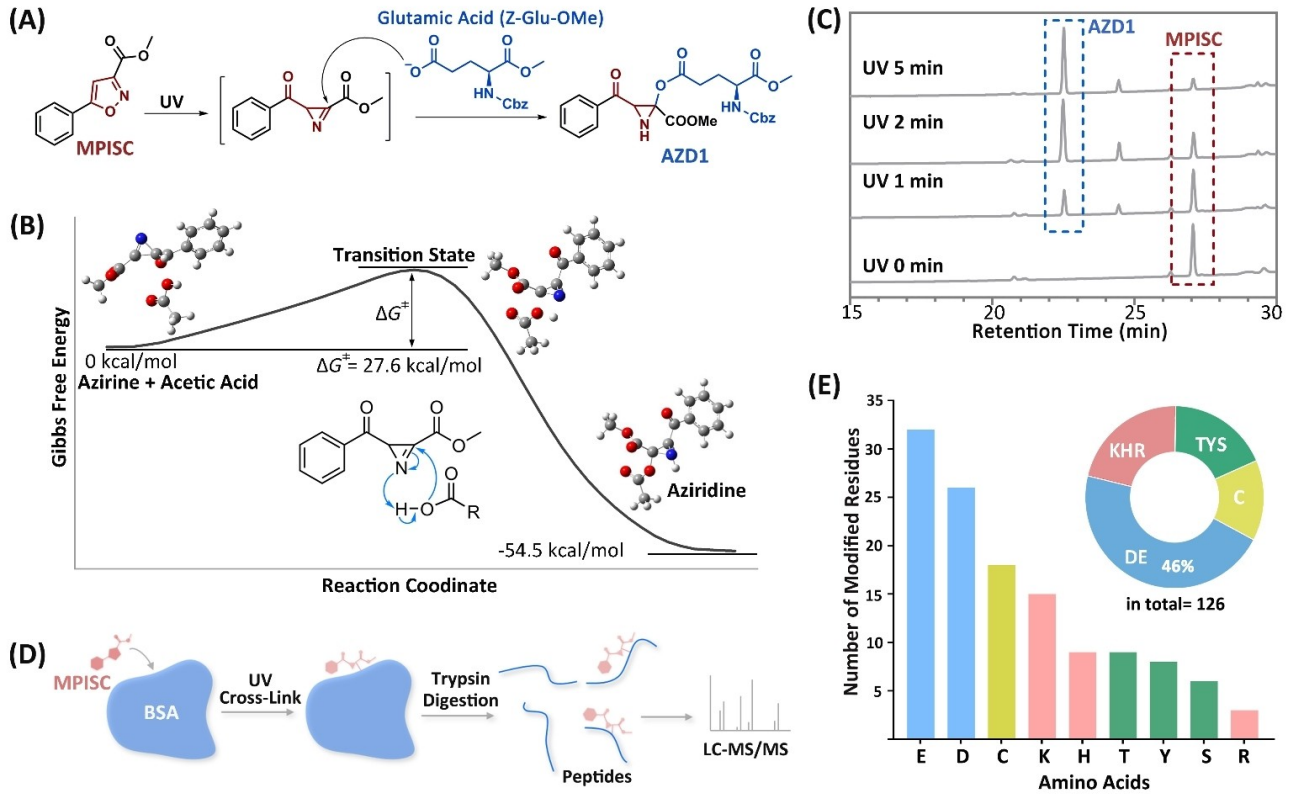

Figure 2. A) Proposed photoreaction mechanism of **MPISC** with glutamic acid. B) Analysis of the reaction coordinate of the azirine intermediate and acetic acid by DFT calculations at B3LYP/6-311+G(d,p) level. C) HPLC analysis of the photoreaction between **MPISC** and glutamic acid in acetonitrile/PBS (1:1, pH 7.4); The reaction was monitored at 254 nm channel. D) Workflow of photo-cross-linking site analysis on BSA. E) Histogram and pie chart analysis of total photo-cross-linking sites on BSA by **MPISC**.

acid, cysteine, and terminal lysine were identified as the exact photo-cross-linking sites (Figure S11a–c). To further investigate the photo-cross-linking reaction of isoxazole and proteins, bovine serum albumin (BSA) was used as a model protein. The workflow is illustrated in Figure 2D. As expected, photo-cross-linking of **MPISC** with various residue types was observed on BSA. Representative residues were resolved to demonstrate the photo-cross-linking on carboxylic residues (E, D; Figure S12a,b), basic residues (R, K, H; Figure S12c–e), hydroxylic residues (Y, S, T; Figure S12f–h), and cysteine (C; Figure S12i). In total, 126 residues were identified as the specific photo-cross-linking sites, summarized in Figure 2E. Interestingly, 46% of the residues are carboxylic amino acids, accounting for the largest proportion. This might be attributed to the higher photoreactivity of isoxazoles towards carboxylic acids. Overall, these results demonstrated the remarkable photo-cross-linking ability of isoxazole towards peptides and protein, providing a solid basis for further proteome labeling and chemoproteomic studies.

Next, a series of functionalized isoxazole probes (**isx1–8**) were designed for in vitro/situ protein labeling (Figure 3A). These probes were decorated with diverse substituents on the five-membered ring of isoxazole, including alkyl, aryl, amine, amide, and trifluoromethyl groups. Meanwhile, a terminal alkyne was introduced to each probe and served as a biorthogonal tag for protein visualization and enrichment. The chemical synthesis of **isx1–8** was carried out by robust coupling and substitution reactions (Scheme S1, S2). For comparison purpose, a non-specific diazirine probe (**DZP**) and a non-specific benzophenone probe (**BZP**) were included to compare the labeling efficiency of isoxazole probes (Figure 3A).

With these isoxazole probes in hand, we next assessed their protein labeling abilities under in vitro/situ conditions. As shown in Figure 3B, a strong fluorescent band around 70 kDa was observed in each lane, suggesting the labeling of BSA by these isoxazole probes. In particular, the aryl-substituted isoxazoles, **isx6–8**, exhibited stronger fluorescence than the alkyl-substituted isoxazoles (**isx1–5**). Meanwhile, the labeling intensity of aryl-substituted isoxazole probes (**isx6–8**) was similar to that of diazirine and benzophenone probes (**DZP** and **BZP**), suggesting their comparable labeling efficiency. UV time-dependent and probe concentration-dependent labeling experiments were performed with **isx6** and BSA to evaluate the photo-cross-linking efficiency. The labeling of BSA by **isx6** was observable in 20 s of UV irradiation, and the intensity enhanced significantly as the irradiation time increased to 300 s (Figure 3C), demonstrating the superior photo-cross-linking efficiency of **isx6**. Meanwhile, the labeling intensity of BSA was dependent on the concentration of **isx6** (Fig-

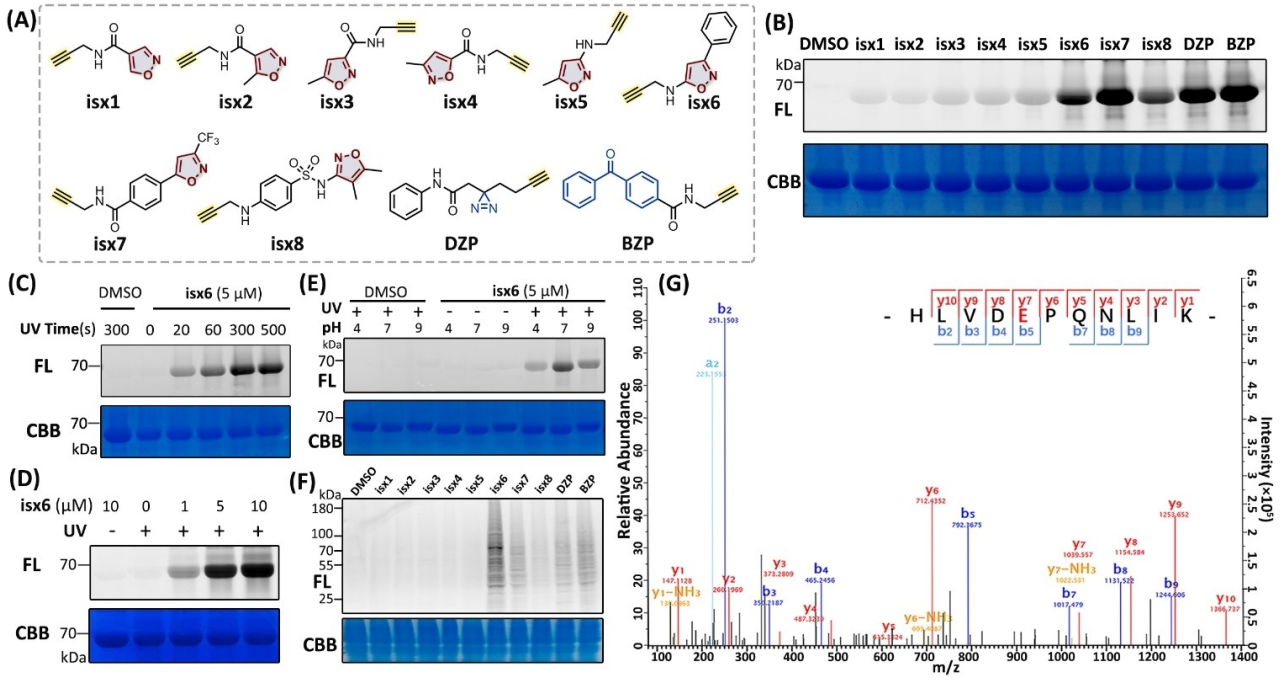

Figure 3. A) Chemical structures of functionalized photoaffinity probes. B) Labeling of BSA with 5 μM of **isx1–8**, **DZP**, and **BZP**; FL: in-gel fluorescence scanning; CBB: coomassie brilliant blue staining. C), D) UV time-dependent/probe concentration-dependent labeling of BSA with **isx6**. E) Labeling of BSA with **isx6** in buffers (Britton-Robinson) with different pHs. F) In situ labeling of 5 μM **isx1–8**, **DZP**, and **BZP** with HeLa cells. G) LC–MS/MS analysis of the photo-cross-linking site of **isx6** with **BSA** at a glutamate residue.

ure 3D), and the labeling reached almost equilibrium by treating 5 μM of **isx6**. Furthermore, **isx6** demonstrated strong ability in labeling other recombinant proteins, including avidin, SIRT5, and esterase (Figure S18). To study the effects of environmental pH on the photo-cross-linking of isoxazole, labeling of BSA with **isx6** was performed in aqueous buffers with different pHs (Figure 3E). The results suggested that the isoxazole exhibited the highest photo-cross-linking efficiency around physiological pH conditions.

In situ proteome labeling was carried out in HeLa cells with **isx1–8** (5 μM**)**. Similarly, the alkyl-substituted isoxazole probes (**isx1–5**) presented faint labeling profiles, whereas the aryl-substituted isoxazole probes, especially **isx6**, demonstrated strong labeling profiles with numerous bands found in gel lanes (Figure 3F). In general, aryl-substituted isoxazole probes achieved comparable labeling efficiency with **DZP** and **BZP**. These results suggested that aryl-substituted isoxazole probes may be more suitable for photoaffinity labeling and chemoproteomic studies, probably due to their stronger UV absorption around 302 nm and higher photoreactivity over alkyl-substituted isoxazoles.

Considering the robust labeling of BSA by **isx6–8**, LC–MS/MS analysis was further performed to discover their photo-cross-linking sites. As expected, hundreds of sites were identified for **isx6–8**, which further demonstrates their excellent photo-cross-linking ability and efficiency. Representative photo-cross-linking residues were resolved and shown in Figure 3G and Figure S13a–i. Likewise, carboxylic residues accounted for the most significant proportion of the total photo-cross-linking sites for **isx6–8** (Figure S14), implying their photo-cross-linking preferences towards carboxylic residues.

Encouraged by the excellent photo-cross-linking efficiency and ability of the isoxazole group, two isoxazole-containing drugs, Danazol and Luminespib, were then applied to integrated chemoproteomic platforms to reveal their cellular targets and drug action mechanisms. Danazol (**isx9**, Figure S1) is an FDA-approved synthetic hormone for treating symptoms such as endometriosis. Although Danazol was lately applied to several clinical studies, its cellular targets remain unclear, and severe side effects on liver, cardiac, and kidney were frequently reported.[13] As Danazol carries a native terminal alkyne, it can be directly applied to chemoproteomics without chemical modification. We first tested the cytotoxicity of Danazol against a normal human embryonic kidney cell line, HEK 293T. As expected, 5 μM Danazol caused significant toxicity to HEK 293T cells (Figure S15). In situ labeling was then performed with Danazol in HEK 293T cells. The labeling profiles showed several strong fluorescent bands distributed in the range of 45–90 kDa (Figure S20), indicating the potential cellular targets of Danazol.

Next, TMT-based quantitative chemoproteomic experiments were performed with Danazol (5 μM) using HEK 293T cells. Overall, 48 protein hits were enriched by the quantitative proteomic analysis as the potential cellular targets of Danazol (Figure S23, Table S1). Although no hormone receptors were detected, probably due to their low abundance, TATA element modulatory factor 1 (TMF1/ARA160) was identified and recognized as the coactivator

of androgen receptor (AR),[14] and P53 was identified and reported as an AR signaling protein and estrogen receptor (ER) binding protein.[15] These results implied the potential hormonal activity of Danazol. Moreover, a series of protein disulfide isomerases (PDI), including PDIA1, PDIA3, PDIA4, and PDIA6, were significantly enriched. Interestingly, PDI was reported as a modulator of hormone receptors, and the inhibition of PDI by hormones such as estrone was reported previously.[16]

We next performed pull-down/western blotting (WB) validation with two proteins enriched by Danazol. As shown in Figure S24, the blotting displayed significant enrichment of intracellular P53 and PDIA1 by 5 μM Danazol, suggesting their potential interactions with Danazol in HEK 293T cells. In addition, a fluorometric PDI activity assay was utilized to test the PDI inhibition of Danazol. Interestingly, Danazol demonstrated considerable inhibition on intracellular PDI, and the inhibitory activity was similar to other hormones (Figure S25). Next, protein-protein interactions of these enriched proteins were analyzed by the STRING database[17] (11.5) and resolved in networks (Figure S26). Significant interactions among PDI, cellular tumor antigen p53 (P53), vimentin (VIM), and other nine proteins were observed. Gene Ontology (GO) enrichment analysis was also performed, and the results demonstrated multiple functions of enriched proteins, including PDI activity and mRNA processing (Figure S27).

The chemoproteomic study of Danazol demonstrated the feasibility of utilizing isoxazole moiety as a native photo-cross-linker. We next moved on to Luminespib (AUY-922), a potent isoxazole-containing Hsp90 inhibitor developed for cancer treatment.[18] Despite its remarkable potency in clinical trials, adverse effects were frequently observed in phase 1/2 studies.[19] Due to safety concerns, Luminespib and many other Hsp90 inhibitors were restricted to clinical trials. Considering the great potential of Hsp90 as a therapeutic target, it is urgent to study the cellular targets and action mechanisms of Hsp90 inhibitors to meet clinical needs.

The binding pattern of Luminespib and Hsp90 (PDB ID: 2VCI) was first examined.[18] The acetamido tail of Luminespib is located outward of the ATP-binding pocket of Hsp90. Hence, the acetamido tail can tolerate certain chemical modifications. When introducing an alkynyl group to this optimal position, most Hsp90 inhibitory activity of Luminespib could be retained (Figure 4A). Consequently, **isx10**, a functionalized Hsp90 probe with a native isoxazole moiety, was designed from Luminespib and synthesized in 10 steps (Scheme S3 ~ S4). Docking analysis was performed to predict the binding of **isx10** to Hsp90. As a result, **isx10** presented similar atomic coordinates and Hsp90-binding patterns to Luminespib (Figure 4B), indicating that **isx10** largely preserved the bioactivity of Luminespib. The IC_{50} values of **isx10** and Luminespib were then measured with various cancer cells. As expected, **isx10** and Luminespib exhibited close IC_{50} against three cancer cell lines (HeLa, A549, and HCT116) (Figure 4C & Figure S16, S17), suggesting that **isx10** is suitable for Hsp90 labeling and chemoproteomic studies.

Hence, **isx10** was applied to proteome labeling with HeLa cells, and Luminespib was used as the competitor. According to the labeling profile, a strong fluorescent labeling band around 90 kDa was observed in the group

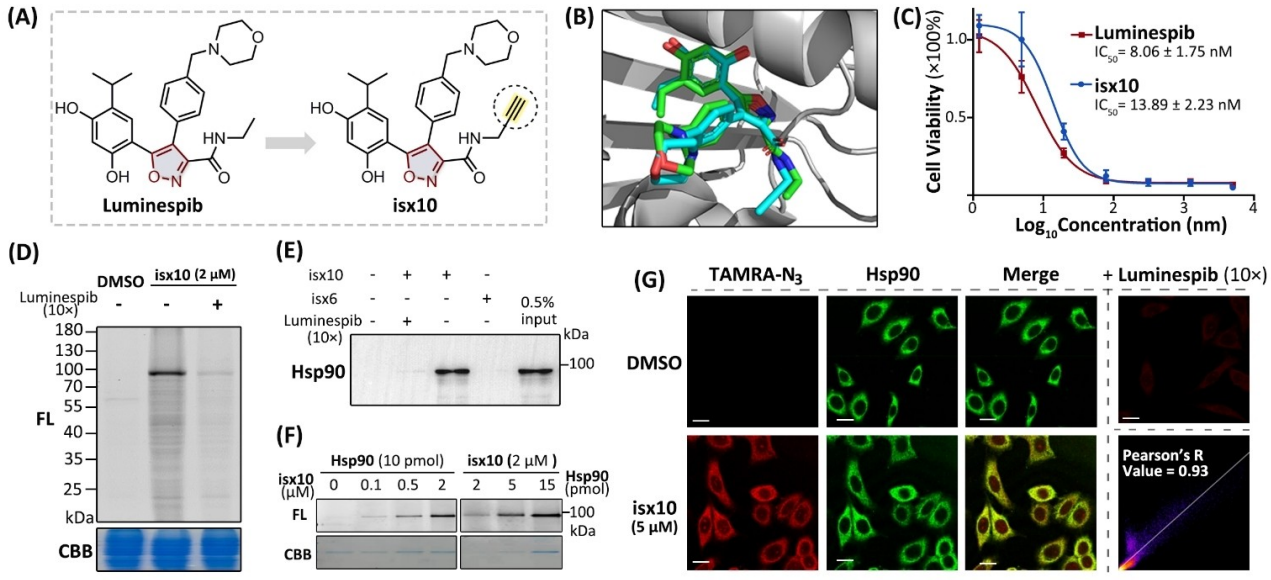

Figure 4. A) Chemical structures of Luminespib and **isx10**. B) Docking analysis of **isx10** and Hsp90. Luminespib, **isx10**, and Hsp90 (2VCI) are shown in green, cyan, and gray, respectively. C) IC_{50} values of Luminespib and **isx10** against HeLa cells; Error bars = standard deviation of the mean, $n = 5$. D) In situ labeling profile of **isx10** (2 μM) with HeLa cells. E) Pull-Down/WB result for target validation of **isx10** (5 μM) with anti-Hsp90. 0.5% input is a loading control representing 0.5% of whole cell lysate. F) Labeling of recombinant Hsp90 with **isx10**. G) Cellular imaging of Hsp90 with **isx10** (5 μM) in HeLa cells. Scale bar = 20 μm. The green fluorescence belongs to the immunofluorescence of Hsp90 and the red fluorescence comes from **isx10**.

treated with 2 μM of **isx10** (Figure 4D), indicating the specific labeling of Hsp90. With the competition by Luminespib (10×), the labeling band was significantly repressed. Meanwhile, several faint fluorescent bands were observed throughout the lane, indicating potential unknown cellular targets of **isx10**. Similarly, in vitro labeling of **isx10** presented a specific Hsp90-labeling profile but with additional non-specific labeling (Figure S21). To verify the specific labeling of Hsp90, pull-down enrichment was performed with 5 μM of **isx10**, followed by WB analysis with anti-Hsp90. The WB result demonstrated strong enrichment of intracellular Hsp90 by **isx10** (Figure 4E), and the enrichment could be competed by Luminespib (10×). To further explore the Hsp90 labeling sensitivity of **isx10**, recombinant Hsp90 was obtained and utilized for gel-based labeling. Surprisingly, the labeling profiles showed that **isx10** could label and detect Hsp90 at a low probe concentration (100 nM) (Figure 4F), and the labeling intensity increased in a linear relationship with the concentration of **isx10** (Figure S19). Meanwhile, low amounts of Hsp90 (2–15 pmol) can be sensitively detected by 2 μM of **isx10**.

Inspired by the gel-based labeling results, **isx10** was next applied to the cellular imaging of Hsp90. Since Hsp90 is highly related to various diseases and often overexpressed in tumors,[20] developing probes for specific imaging of intracellular Hsp90 could facilitate cancer diagnosis and treatment. Previous strategies directly modified Hsp90 inhibitors with bulky fluorophores via extra linkers,[21] which may lead to poor permeability and low specificity. In comparison, **isx10** retains most of Hsp90 activity by minimal modification of Luminespib. As shown in Figure 4G & Figure S22, red fluorescence representing the distribution of **isx10** was observed in the cytoplasm of **isx10**-treated cells. The fluorescence intensity increased when the concentration of **isx10** increased and could be abolished by Luminespib (10×). Moreover, the fluorescence of **isx10** overlapped significantly with the immunofluorescence of anti-Hsp90. The Pearson correlation coefficient was calculated to be as high as 0.93. These results together demonstrated the excellent specificity and sensitivity of **isx10** in labeling and imaging native intracellular Hsp90.

Next, **isx10** was employed in TMT-based quantitative chemoproteomic experiments to uncover its cellular targets and interactions. Two sets of chemoproteomic experiments were performed with HeLa cells (**isx10**/DMSO and **isx10**/**isx10**+Luminespib). The chemoproteomic results were resolved and shown in tables and volcano plots (Table S2, S3, Figure 5A, B). Overall, 10 proteins, including Hsp90, nuclear autoantigenic sperm protein (NASP), integrin beta-1 (ITGB1), and prostaglandin E synthase 2 (PTGES2), were enriched under a specific criterion (enrichment fold ≥ 1.5 and p-value < 0.05). Among these proteins, Hsp90, NASP, and other three proteins were enriched in both two sets of chemoproteomic experiments. In particular, NASP is a histone chaperone and Hsp90 binding protein,[22] while ITGB1 is a vital membrane receptor highly associated with cell signaling.[23] Interestingly, PTGES2, an isomerase involved in prostaglandin E2 metabolism, was recently developed as a promising therapeutic target for COVID-19 treatment.[24] It is noted that Antolin et al. recently revealed several kinases as potential off-targets of Luminespib,[25] demonstrating the significance of unique kinase polypharmacology in developing Hsp90 inhibitors. On the other hand, kinases were not prominently enriched in our chemoproteomic experiments. This might be attributed to the lower protein abundance and weaker affinity of kinases with Luminespib under native conditions.

The interactions of these proteins were analyzed with the STRING database. Interactions between Hsp90, NASP, thioredoxin (TXN), and PTGES2 were observed (Figure 5C). Given the potent anti-cancer activity of Luminespib, the gene expression of these targets in normal and tumor tissues was analyzed with a web server, GEPIA (gene expression profiling interactive analysis),[26] to interpret its therapeutic and toxic effects. The tissue types were chosen based on the cancers treated with Luminespib in clinical trials. As shown in Figure 5D, Hsp90 and TXN exhibited higher expression levels in tumor tissues than in normal tissues, which might contribute to the cancer therapeutic specificity of Luminespib. In comparison, other genes displayed no significant difference in tumor and normal tissues, indicating the potential toxicity and side effects associated with these genes.

Next, cellular thermal shift assay (CETSA) was performed to validate these targets. The thermal melting curves of NASP and PTGES2 were plotted based on WB analysis of the soluble proteins at different temperatures (Figure 5E, F & Figure S28, S29). With the addition of Luminespib, the melting curve of NASP shifted right, reflecting the melting temperature increase induced by the thermal stabilization of NASP by Luminespib. Likewise, the melting curve of PTGES2 shifted right with the treatment of Luminespib or indomethacin (a PTGES2 inhibitor), indicating their binding to PTGES2. Pull-down/WB experiments were further performed with **isx10** and the corresponding antibodies. The results demonstrated prominent enrichment of NASP, PTGES2, and ITGB1 by 5 μM of **isx10** (Figure 5G), and the enrichment could be significantly repressed by Luminespib (10×) or indomethacin (10×), suggesting the potential interactions of these proteins with **isx10** in cells.

Lastly, inspired by the recently reported covalent inhibition of Hsp90 in Hamachi and Taunton's work,[27] we next investigated the plausibility of Luminespib for covalent inhibition of Hsp90 triggered by UV. This strategy may expand the application of isoxazole-containing drugs and offer new opportunities for developing photo-triggered drugs. We first performed the cell viability assay to estimate the cellular effects caused by covalent inhibition of Luminespib under UV irradiation. With the pre-treatment of Luminespib (4 h followed by washout), no UV-treated groups displayed minor cytotoxicity (Figure 5H), likely due to the washout of Luminespib. In contrast, with the treatment of Luminespib and UV irradiation, high cytotoxicity was observed, indicating the toxic effects caused by the irreversible binding of Hsp90. WB analysis was then conducted to assess the cellular function at molecular levels under the covalent inhibition of Hsp90. Interestingly, the levels of Hsp90 client proteins, including HER2, c-Raf, and

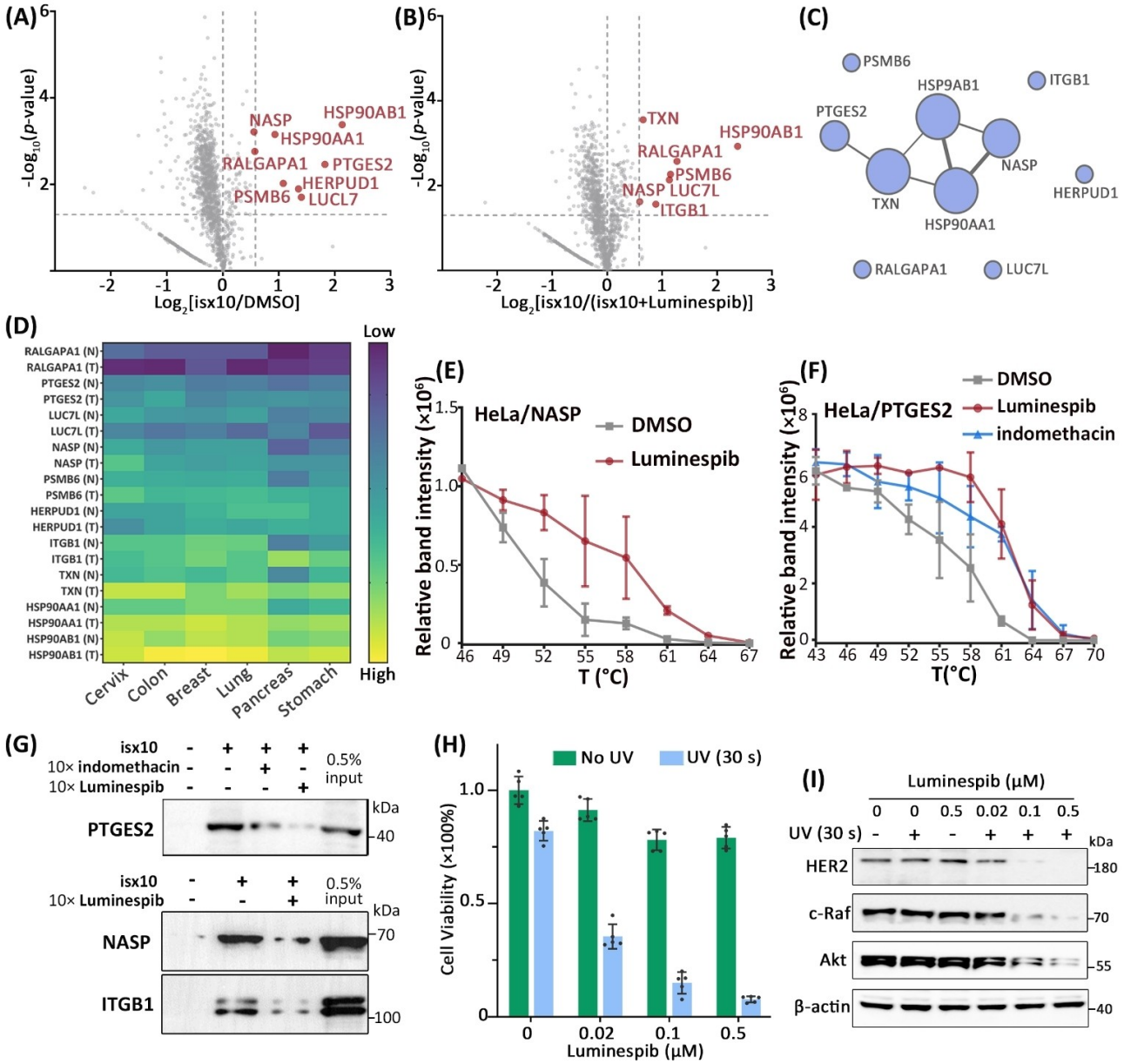

Figure 5. A), B) Proteins enriched by **isx10** (5 μM) in the presence or absence of Luminespib with HeLa cells, shown in volcano plots; Red dots represent qualified protein hits; Chemoproteomic experiments were performed in three replicates. C) Protein-protein interactions of the proteins identified in (A)&(B). Minimum required interaction score: 0.4; Line thickness indicates the correlation between nodes. D) Gene expression analysis of identified proteins in tumor (T) and normal (N) tissue, based on the UCSC Xena project (http://xena.ucsc.edu). E), F) Thermal melting curves of NASP and PTGES2 with/without treating Luminespib (5 μM) or indomethacin (5 μM); Error bars = standard deviation of the mean, $n = 3$. G) Pull-down/WB results for targets validation of **isx10** (5 μM) in HeLa cells. H) Cell viability (HeLa) by pre-treatment of Luminespib, with/without UV irradiation; Error bars = standard deviation of the mean, $n = 5$. I) WB analysis of Hsp90 client proteins in HeLa cells under treatment of Luminespib and UV irradiation.

Akt, decreased significantly under the pre-treatment of Luminespib and UV irradiation (Figure 5I), suggesting the destabilization of these client proteins induced by the covalent inhibition of Hsp90 chaperone activity. Hence, this could explain the increased cytotoxicity observed under pre-treatment of Luminespib and UV irradiation.

Conclusion

In conclusion, we have successfully developed the isoxazole group, a common pharmacophore, into a novel photo-cross-linker. The photochemistry of isoxazole with amino acids, peptides, and proteins has been studied in detail for the first time. In vitro/situ protein labeling of functionalized isoxazole probes demonstrated the excellent ability and efficiency of isoxazoles as photo-cross-linkers. Chemopro-

teomic studies with two isoxazole-containing drugs, Danazol and Luminespib, revealed their potential cellular targets and interactions. Potential protein targets, including TMF1, P53, and PDI, were identified for Danazol. In particular, Danazol was verified with PDI inhibitory activity, implying that PDI is likely a valid target for Danazol. Meanwhile, **isx10**, a powerful probe derived from Luminespib, was successfully developed for proteome labeling, cellular imaging, and chemoproteomic studies. **isx10** exhibited superior sensitivity and specificity in labeling and imaging native intracellular Hsp90. Chemoproteomic studies of **isx10** revealed Hsp90 as a primary cellular target, and other potential targets, including NASP, a protein chaperone, and PTGES2, a promising antiviral target for COVID-19 treatment. Furthermore, Luminespib was investigated for covalent inhibition towards Hsp90 under UV irradiation. We anticipate these results and findings will contribute to the development of isoxazole-based drugs and benefit future disease diagnoses and therapeutics.

Acknowledgements

The authors thank the financial support from the National Natural Science Excellent Young Scientists Fund of China (Hong Kong and Macau) (Grant No. 32122003), Research Grants Council of Hong Kong (Grant Nos. 11302320 and 11305221). We thank Prof. Deng Wenbin for his invaluable suggestions on this work.

Conflict of Interest

The authors declare no conflict of interest.

Data Availability Statement

The data that support the findings of this study are available from the corresponding author upon reasonable request.

Keywords: Chemoproteomics · Drug Discovery · Isoxazole · Photo-Cross-Linker · Photoaffinity Labeling

[1] a) Y. Xia, L. Peng, *Chem. Rev.* **2013**, *113*, 7880–7929; b) M. H. Wright, S. A. Sieber, *Nat. Prod. Rep.* **2016**, *33*, 681–708; c) J. R. Hill, A. A. B. Robertson, *J. Med. Chem.* **2018**, *61*, 6945–6963; d) Y. Zhang, T. G. Kutateladze, *Nat. Chem.* **2020**, *12*, 506–508; e) W. Yu, J. M. Baskin, *Curr. Opin. Chem. Biol.* **2022**, *69*, 102173.

[2] a) C. G. Parker, A. Galmozzi, Y. Wang, B. E. Correia, K. Sasaki, C. M. Joslyn, A. S. Kim, C. L. Cavallaro, R. M. Lawrence, S. R. Johnson, I. Narvaiza, E. Saez, B. F. Cravatt, *Cell* **2017**, *168*, 527–541; b) J. Gao, A. Mfuh, Y. Amako, C. M. Woo, *J. Am. Chem. Soc.* **2018**, *140*, 4259–4268; c) Y. Xie, L. Chen, R. Wang, J. Wang, J. Li, W. Xu, Y. Li, S. Q. Yao, L. Zhang, Q. Hao, H. Sun, *J. Am. Chem. Soc.* **2019**, *141*, 18428–18436; d) H. A. Flaxman, C. F. Chang, H. Y. Wu, C. H. Nakamoto, C. M. Woo, *J. Am. Chem. Soc.* **2019**, *141*, 11759–11764; e) H. Su, J. Xu, Y. Chen, Q. Wang, Z. Lu, Y. Chen, K. Chen, S. Han, Z. Fang, P. Wang, B. F. Yuan, X. Zhou, *J. Am. Chem. Soc.* **2021**, *143*, 1917–1923; f) F. Tzakoniati, H. Xu, T. Li, N. Garcia, C. Kugel, J. Payandeh, C. M. Koth, E. W. Tate, *Cell Chem. Biol.* **2020**, *27*, 306–313; g) J. Sileikyte, S. Sundalam, L. L. David, M. S. Cohen, *J. Am. Chem. Soc.* **2021**, *143*, 6787–6791; h) T. A. Nguyen, T. Gronauer, T. Nast-Kolb, S. Sieber, K. Lang, *Angew. Chem. Int. Ed.* **2022**, *61*, e202111085; *Angew. Chem.* **2022**, *134*, e202111085; i) C. A. Weidmann, A. M. Mustoe, P. B. Jariwala, J. M. Calabrese, K. M. Weeks, *Nat. Biotechnol.* **2021**, *39*, 347–356.

[3] M. W. Halloran, J. P. Lumb, *Chem. Eur. J.* **2019**, *25*, 4885–4898.

[4] Z. Li, P. Hao, L. Li, C. Y. Tan, X. Cheng, G. Y. Chen, S. K. Sze, H. M. Shen, S. Q. Yao, *Angew. Chem. Int. Ed.* **2013**, *52*, 8551–8556; *Angew. Chem.* **2013**, *125*, 8713–8718.

[5] Z. Li, L. Qian, L. Li, J. C. Bernhammer, H. V. Huynh, J. S. Lee, S. Q. Yao, *Angew. Chem. Int. Ed.* **2016**, *55*, 2002–2006; *Angew. Chem.* **2016**, *128*, 2042–2046.

[6] Y. Zou, L. Liu, J. Liu, G. Liu, *Future Med. Chem.* **2020**, *12*, 91–93.

[7] a) K. Cheng, J. S. Lee, P. Hao, S. Q. Yao, K. Ding, Z. Li, *Angew. Chem. Int. Ed.* **2017**, *56*, 15044–15048; *Angew. Chem.* **2017**, *129*, 15240–15244; b) N. Ma, Z. M. Zhang, J. S. Lee, K. Cheng, L. Lin, D. M. Zhang, P. Hao, K. Ding, W. C. Ye, Z. Li, *ACS Chem. Biol.* **2019**, *14*, 2546–2552.

[8] W. Zhao, A. R. Cross, C. Crowe-McAuliffe, A. Weigert-Munoz, E. E. Csatary, A. E. Solinski, J. Krysiak, J. B. Goldberg, D. N. Wilson, E. Medina, W. M. Wuest, S. A. Sieber, *Angew. Chem. Int. Ed.* **2019**, *58*, 8581–8584; *Angew. Chem.* **2019**, *131*, 8670–8674.

[9] a) E. F. Ullman, B. Singh, *J. Am. Chem. Soc.* **1966**, *88*, 1844–1845; b) C. M. Nunes, I. Reva, R. Fausto, *J. Org. Chem.* **2013**, *78*, 10657–10665; c) S. Pusch, T. Opatz, *Org. Lett.* **2014**, *16*, 5430–5433; d) S. Pusch, D. Kowalczyk, T. Opatz, *J. Org. Chem.* **2016**, *81*, 4170–4178.

[10] a) Q. Peng, D. Guo, J. Bie, J. Wang, *Angew. Chem. Int. Ed.* **2018**, *57*, 3767–3771; *Angew. Chem.* **2018**, *130*, 3829–3833; b) S. Nakamura, D. Hayama, M. Miura, T. Hatanaka, Y. Funahashi, *Org. Lett.* **2018**, *20*, 856–859; c) A. F. Khlebnikov, M. S. Novikov, N. V. Rostovskii, *Tetrahedron* **2019**, *75*, 2555–2624; d) N. Ma, J. Hu, Z. M. Zhang, W. Liu, M. Huang, Y. Fan, X. Yin, J. Wang, K. Ding, W. Ye, Z. Li, *J. Am. Chem. Soc.* **2020**, *142*, 6051–6059; e) Y. Chen, W. Yang, J. Wu, W. Sun, T. P. Loh, Y. Jiang, *Org. Lett.* **2020**, *22*, 2038–2043.

[11] a) G. C. Arya, K. Kaur, V. Jaitak, *Eur. J. Med. Chem.* **2021**, *221*, 113511; b) A. Sysak, B. Obminska-Mrukowicz, *Eur. J. Med. Chem.* **2017**, *137*, 292–309.

[12] a) J. Zhu, J. Mo, H. Z. Lin, Y. Chen, H. P. Sun, *Bioorg. Med. Chem.* **2018**, *26*, 3065–3075; b) N. Agrawal, P. Mishra, *Med. Chem. Res.* **2018**, *27*, 1309–1344.

[13] a) D. M. Townsley, B. Dumitriu, D. Liu, A. Biancotto, B. Weinstein, C. Chen, N. Hardy, A. D. Mihalek, S. Lingala, Y. J. Kim, J. Yao, E. Jones, B. R. Gochuico, T. Heller, C. O. Wu, R. T. Calado, P. Scheinberg, N. S. Young, *N. Engl. J. Med.* **2016**, *374*, 1922–1931; b) P. R. Colunga-Pedraza, J. E. Colunga-Pedraza, M. A. Garza-Ledezma, J. C. Jaime-Perez, O. G. Cantu-Rodriguez, C. H. Gutierrez-Aguirre, E. J. Rendon-Ramirez, Y. K. Lopez-Garcia, R. E. Lozano-Morales, A. Gomez-De Leon, G. Sotomayor-Duque, D. Gomez-Almaguer, *Clin. Lymphoma Myeloma* **2018**, *18*, e109-e113; c) A. Garcia-Horton, Y. Valliere, A. Lazo-Langner, *Leuk. Res.* **2020**, *94*, 106370.

[14] a) P. W. Hsiao, C. Chang, *J. Biol. Chem.* **1999**, *274*, 22373–22379; b) H. V. Heemers, D. J. Tindall, *Endocr. Rev.* **2007**, *28*, 778–808; c) H. V. Heemers, K. M. Regan, L. J. Schmidt, S. K. Anderson, K. V. Ballman, D. J. Tindall, *Mol. Endocrinol.* **2009**, *23*, 572–583.

[15] a) M. V. Cronauer, W. A. Schulz, T. Burchardt, R. Ackermann, M. Burchardt, *Oncogene* **2004**, *23*, 3541–3549; b) W. Liu, S. D. Konduri, S. Bansal, B. K. Nayak, S. A. Rajasekaran, S. M. Karuppayil, A. K. Rajasekaran, G. M. Das, *J. Biol. Chem.* **2006**, *281*, 9837–9840; c) S. D. Konduri, R. Medisetty, W. Liu, B. A. Kaipparettu, P. Srivastava, H. Brauch, P. Fritz, W. M. Swetzig, A. E. Gardner, S. A. Khan, G. M. Das, *Proc. Natl. Acad. Sci. USA* **2010**, *107*, 15081–15086.

[16] a) J. C. Tsibris, L. T. Hunt, G. Ballejo, W. C. Barker, L. J. Toney, W. N. Spellacy, *J. Biol. Chem.* **1989**, *264*, 13967–13970; b) T. P. Primm, H. F. Gilbert, *J. Biol. Chem.* **2001**, *276*, 281–286; c) X. M. Fu, P. Wang, B. T. Zhu, *Biochemistry* **2011**, *50*, 106–115; d) M. M. G. Khan, S. Simizu, N. S. Lai, M. Kawatani, T. Shimizu, H. Osada, *ACS Chem. Biol.* **2011**, *6*, 245–251; e) S. R. Fernando, C. L. Lee, B. P. Wong, K. W. Cheng, Y. L. Lee, M. C. Chan, E. H. Ng, W. S. Yeung, K. F. Lee, *Exp. Cell Res.* **2021**, *405*, 112665.

[17] D. Szklarczyk, A. L. Gable, K. C. Nastou, D. Lyon, R. Kirsch, S. Pyysalo, N. T. Doncheva, M. Legeay, T. Fang, P. Bork, L. J. Jensen, C. von Mering, *Nucleic Acids Res.* **2021**, *49*, D605–D612.

[18] P. A. Brough, W. Aherne, X. Barril, J. Borgognoni, K. Boxall, J. E. Cansfield, K. M. Cheung, I. Collins, N. G. Davies, M. J. Drysdale, B. Dymock, S. A. Eccles, H. Finch, A. Fink, A. Hayes, R. Howes, R. E. Hubbard, K. James, A. M. Jordan, A. Lockie, V. Martins, A. Massey, T. P. Matthews, E. McDonald, C. J. Northfield, L. H. Pearl, C. Prodromou, S. Ray, F. I. Raynaud, S. D. Roughley, S. Y. Sharp, A. Surgenor, D. L. Walmsley, P. Webb, M. Wood, P. Workman, L. Wright, *J. Med. Chem.* **2008**, *51*, 196–218.

[19] a) C. Sessa, G. I. Shapiro, K. N. Bhalla, C. Britten, K. S. Jacks, M. Mita, V. Papadimitrakopoulou, T. Pluard, T. A. Samuel, M. Akimov, C. Quadt, C. Fernandez-Ibarra, H. Lu, S. Bailey, S. Chica, U. Banerji, *Clin. Cancer Res.* **2013**, *19*, 3671–3680; b) S. B. Gaykema, C. P. Schroder, J. Vitfell-Rasmussen, S. Chua, T. H. Oude Munnink, A. H. Brouwers, A. H. Bongaerts, M. Akimov, C. Fernandez-Ibarra, M. N. Lub-de Hooge, E. G. de Vries, C. Swanton, U. Banerji, *Clin. Cancer Res.* **2014**, *20*, 3945–3954; c) R. Seggewiss-Bernhardt, R. C. Bargou, Y. T. Goh, A. K. Stewart, A. Spencer, A. Alegre, J. Blade, O. G. Ottmann, C. Fernandez-Ibarra, H. Lu, S. Pain, M. Akimov, S. P. Iyer, *Cancer* **2015**, *121*, 2185–2192.

[20] L. Whitesell, S. L. Lindquist, *Nat. Rev. Cancer* **2005**, *5*, 761–772.

[21] L. B. Crowe, P. F. Hughes, D. A. Alcorta, T. Osada, A. P. Smith, J. Totzke, D. R. Loiselle, I. D. Lutz, M. Gargesha, D. Roy, J. Roques, D. Darr, H. K. Lyerly, N. L. Spector, T. A. J. Haystead, *ACS Chem. Biol.* **2017**, *12*, 1047–1055.

[22] a) C. P. Liu, W. Jin, J. Hu, M. Wang, J. Chen, G. Li, R. M. Xu, *Genes Dev.* **2021**, *35*, 1610–1624; b) O. M. Alekseev, E. E. Widgren, R. T. Richardson, M. G. O'Rand, *J. Biol. Chem.* **2005**, *280*, 2904–2911.

[23] T. Arimori, N. Miyazaki, E. Mihara, M. Takizawa, Y. Taniguchi, C. Cabanas, K. Sekiguchi, J. Takagi, *Nat. Commun.* **2021**, *12*, 4012.

[24] a) D. E. Gordon, G. M. Jang, M. Bouhaddou, J. Xu, K. Obernier, K. M. White, M. J. O'Meara, V. V. Rezelj, J. Z. Guo, D. L. Swaney, et al., *Nature* **2020**, *583*, 459–468; b) D. E. Gordon, J. Hiatt, M. Bouhaddou, V. V. Rezelj, S. Ulferts, H. Braberg, A. S. Jureka, K. Obernier, J. Z. Guo, J. Batra, et al., *Science* **2020**, *370*, eabe9403; c) J. Desantis, B. Mercorelli, M. Celegato, F. Croci, A. Bazzacco, M. Baroni, L. Siragusa, G. Cruciani, A. Loregian, L. Goracci, *Eur. J. Med. Chem.* **2021**, *226*, 113814.

[25] A. A. Antolin, P. A. Clarke, I. Collins, P. Workman, B. Al-Lazikani, *Cell Chem. Biol.* **2021**, *28*, 1433–1445.

[26] Z. Tang, C. Li, B. Kang, G. Gao, C. Li, Z. Zhang, *Nucleic Acids Res.* **2017**, *45*, W98–W102.

[27] a) T. Tamura, T. Ueda, T. Goto, T. Tsukidate, Y. Shapira, Y. Nishikawa, A. Fujisawa, I. Hamachi, *Nat. Commun.* **2018**, *9*, 1870; b) A. Cuesta, X. Wan, A. L. Burlingame, J. Taunton, *J. Am. Chem. Soc.* **2020**, *142*, 3392–3400.

Manuscript received: July 7, 2022
Accepted manuscript online: September 23, 2022
Version of record online: October 19, 2022